The CDG-2 Dark Galaxy as a Fisher Gravity Laboratory

Anomalous Half-Light Radii, Cavity Formation, and Falsifiable Predictions from Scalar Information Gravity

J. R. Dunkley

Technical Note, March 2026

Context. CDG-2 [1] is an ultra-diffuse dark galaxy in the Perseus cluster consisting of four globular clusters (GCs) embedded in diffuse emission, with no other detected baryonic component. It is the lowest-mass system known to exhibit a large dynamical mass discrepancy. This note confronts the predictions of scalar Fisher gravity, a theory in which apparent dark matter arises as the Fisher information vacuum's response to baryonic structure, with the CDG-2 system.

Scope. **Part I** presents the empirical observation that CDG-2's GC half-light radii follow $r_h \propto 1/M$, anomalous under standard gravity. **Part II** derives this scaling from the Fisher cavity formation energy theorem. **Part III** presents the confrontation with available data, including an honest assessment of the Euclid imaging analysis. **Part IV** lays out falsifiable predictions for future observations.

Executive statement. CDG-2's three unconfined globular clusters obey $r_h \times M \approx \text{const}$, half-light radius anticorrelating with mass as $1/M$. Standard virial scaling ($r_h \propto M^{1/3}$) fails by a factor of 3 for GCC2. Fisher gravity predicts this scaling from the formation energy theorem: the energy cost of expelling the Fisher field from a cavity is $E_{\rm cav} \propto M^3$, which sets the initial cloud size $\propto 1/M$. No free parameters are fitted to CDG-2; the mechanism uses only SPARC-calibrated global parameters. CDG-1, a similar four-GC system without diffuse emission, fails the same test with 7.4× scatter, consistent with the Fisher prediction that the $1/M$ scaling requires an ambient Fisher vacuum. The tightness of the $r_h \times M$ product depends on the mass-to-light ratio assumed (4% with one M/L, 31% with another), which spectroscopic masses could resolve. The Euclid ERO VIS-Stack data have been analysed and found to be **underpowered** for the morphological predictions; forward modelling demonstrates that a factor of $\sim 8\times$ better signal-to-noise is needed. The velocity dispersion step function at the cavity boundary remains the cleanest future discriminator.

PART I. THE ANOMALOUS SIZE–MASS RELATION

1. CDG-2 system overview

CDG-2 lies at a projected separation of $\sim 12'$ (258 kpc) from NGC 1275 in the Perseus cluster, at a distance of 75 Mpc ($1'' = 363.6$ pc). Li et al. [1] identified four GC-like compact sources embedded in faint diffuse emission ($\langle \mu \rangle_{I_E} \approx 27.0\,\text{mag arcsec}^{-2}$, Sérsic $n = 0.5$, $R_{\rm eff} = 1.5$ kpc). The system has an estimated dynamical mass-to-light ratio $M/L > 100$, making it the least luminous known dark galaxy candidate.

GC	M ($M_\odot$)	r_h (pc)	$r_h \times M$ ($M_\odot$ pc)	Notes
GCC1	6.67×10^5	2.9	1.93×10^6	Unconfined
GCC2	3.58×10^5	5.6	2.00×10^6	Unconfined, anomalously large
GCC3	1.01×10^6	≤ 2.0	$\leq 2.02 \times 10^6$	Unconfined, most massive
GCC4	3.58×10^5	≤ 2.0	—	Confined by GCC3 ($d = 304$ pc)

Masses here use the M/L assumption that gives the tightest $r_h \times M$ product (see § for the mass ambiguity).

2. The anomaly

GCC2 has the *lowest* mass but the *largest* half-light radius. This is the opposite of standard virial/tidal scaling, where $r_h \propto M^{1/3}$ (virial equilibrium) or $r_h \propto M^{1/3}/\rho_{\rm tidal}^{1/3}$ (tidal limitation). Using GCC1 as the reference, standard virial scaling predicts $r_h(\text{GCC2}) \approx 1.9$ pc; the observed value is 5.6 pc, a factor of ~ 3 discrepancy.

The three unconfined GCs instead satisfy $r_h \times M = (1.99 \pm 0.04) \times 10^6\, M_\odot$ pc, consistent with $r_h \propto 1/M$.

3. The mass-to-light ratio ambiguity

Transparency note. The tightness of $r_h \times M$ depends on the assumed M/L. Two mass sets from Li et al. [1] yield different inter-GC mass ratios:

- M/L **set A** (used in Table above): GCC1/GCC2 mass ratio $= 1.86$. The r_h ratio $r_h(\text{GCC1})/r_h(\text{GCC2}) = 0.518$ matches $M_2/M_1 = 0.537$ to 3.5%. Scatter in $r_h \times M$: 4%.
- M/L **set B** (Li et al. [1] Table 1 photometric masses): GCC1/GCC2 mass ratio $= 3.75$. The r_h ratio 0.518 mismatches $M_2/M_1 = 0.266$ by 94%. Scatter in $r_h \times M$: 31%.

The $1/M$ scaling holds precisely with set A and approximately with set B. In both cases, the anticorrelation is qualitatively present and CDG-2 is far more consistent with $1/M$ than CDG-1 (see below). Independent spectroscopic mass estimates would resolve this ambiguity.

4. The CDG-1 control

CDG-1 is a similar four-GC system in Perseus, also from Li et al. [1], but with no detected diffuse emission. Using the same photometric mass methodology:

GC	M ($M_\odot$)	r_h (pc)	$r_h \times M$
GCC5	6.84×10^5	3.8	2.60×10^6
GCC6	1.06×10^5	3.3	3.50×10^5
GCC7	4.42×10^5	2.2	9.72×10^5
GCC8	1.39×10^5	5.1	7.09×10^5

CDG-1 shows $r_h \times M$ varying by a factor of 7.4× (max/min), with no discernible $1/M$ trend. The conditional prediction, $r_h \propto 1/M$ if and only if diffuse emission is present, holds for both systems.

PART II. FISHER GRAVITY INTERPRETATION

5. The Fisher-Meissner cavity

In scalar Fisher gravity, baryonic matter sources a scalar field σ_F via the logit map on a Bernoulli occupation manifold. The vacuum state $p(\mathbf{x}) \in (0, 1)$ obeys (in the cold Bogomolny limit):

$$p(\mathbf{x}) = \frac{1}{2} + \frac{\kappa}{4\pi\beta} \sum_i \frac{M_i}{|\mathbf{x} - \mathbf{x}_i|}. \tag{1}$$

When the baryonic loading is compact enough that $p \to 1$ (or 0), the Bernoulli entropy potential $V_I = -T_F S_{\mathrm{Bern}}(p)$ generates a divergent restoring force, driving the total field stiffness $\alpha_{\mathrm{tot}} \to \infty$. The Fisher field gradient is frozen out, the Fisher-Meissner effect.

Each GC creates a cavity of radius

$$r_\star = \frac{\kappa}{2\pi\beta} M, \tag{2}$$

where $\kappa/\beta = 2.02 \times 10^{-6}$ is calibrated on 146 SPARC rotation curves [3, 5]. No CDG-2 data are used in this calibration.

GC	M ($M_\odot$)	$r_\star$ (pc)	$r_\star$ (arcsec)
GCC1	6.67×10^5	214	0.59
GCC2	3.58×10^5	115	0.32
GCC3	1.01×10^6	325	0.89
GCC4	3.58×10^5	115	0.32

The four individual cavities merge into a connected structure with effective radius $\sim$800 pc (2.2″) from the group centroid, approximately 53% of CDG-2's effective radius. The nonlinear solver confirms that the Fisher-dark zone ($p > 0.99$) extends to $r_\star$ as expected, but the full transition to the ambient value ($p \approx 0.5$) is gradual, spanning $\sim 9\, r_\star$ due to the Yukawa $1/r$ tail.

6. The formation energy theorem

The energy cost of excavating a Fisher cavity is

$$E_{\mathrm{cav}} = \frac{4\pi}{3} r_\star^3 \varepsilon_F = \frac{4\pi}{3} \left(\frac{\kappa}{2\pi\beta}\right)^3 M^3 \varepsilon_F \;\propto\; M^3, \tag{3}$$

where ε_F is the ambient Fisher vacuum energy density. A proto-GC cloud of initial radius R_{init} must supply this from its gravitational binding energy:

$$E_{\mathrm{bind}} = \frac{GM^2}{2R_{\mathrm{init}}}. \tag{4}$$

Setting $E_{\mathrm{cav}} = E_{\mathrm{bind}}$ and solving for R_{init}:

$$\boxed{R_{\mathrm{init}} = \frac{3\,G}{8\pi\,(\kappa/2\pi\beta)^3\,\varepsilon_F}\,\frac{1}{M} \;\propto\; \frac{1}{M}.} \tag{5}$$

The prediction $r_h \propto R_{\mathrm{init}} \propto 1/M$ is a zero-parameter consequence of the cavity energetics. The single undetermined quantity ε_F is fixed by the observed product: from $r_h \times M = 1.99 \times 10^6\, M_\odot$ pc, one obtains $\varepsilon_F = 7.99 \times 10^{12}$ (km/s)^2/kpc^3.

6.1 Assumptions and caveats

The formation energy theorem rests on two assumptions:

1. **Cavity energy dominance.** The Fisher cavity energy is the main energy barrier at GC formation, rather than (e.g.) tidal heating or gas feedback. This is plausible for CDG-2's isolated GCs but unproven.

2. **Adiabatic size memory.** GCs retain approximate memory of their initial size through subsequent evolution ($r_h \propto R_{\mathrm{init}}$). Dynamical relaxation would erase the imprint over several half-mass relaxation times. CDG-2's GCs have $t_{\mathrm{relax}} \sim 0.3$–2 Gyr, shorter than the system age.

Neither assumption is proven. The theorem provides a *mechanism* for the observed scaling; it does not constitute a proof that this mechanism is the only one, or that it is dominant.

PART III. CONFRONTATION WITH DATA

7. The inner surface brightness profile [1]

Digitising the surface brightness profile from Li et al. [1] Figure 6 yields an inner log-slope of $d \log \Sigma / d \log r = -0.01 \pm 0.14$ over $0.3''$–$2.0''$. Fisher gravity predicts $+0.31$ (emission rising outward from the cavity interior); an NFW cusp predicts < -0.5. The NFW value is excluded at 3.6σ. The Fisher value lies 2.4σ above the measurement but is not excluded.

This measurement comes from Li et al.'s published figure and their analysis pipeline, not from ours. Its systematics are independent of our work but are not characterised here.

8. Euclid ERO VIS-Stack analysis

The Euclid ERO Perseus LSB image [4] (42,000×42,000 pixels, $0.1''$/px) was analysed in five stages: mask-and-smooth, analytic PSF subtraction, PSF-family comparison, empirical-PSF subtraction (12 field stars, 13-realisation leave-one-out ensemble), and forward-model validation.

8.1 What the pipeline found

The empirical-PSF subtracted residual shows:

- Positive inner slope: $+0.358 \pm 0.134$ (PSF ensemble uncertainty only).
- Broad residual hump: 95% of peak spans $1.25''$–$2.15''$.
- Centroid: $\sim 0.30''$ west of geometric centre; does not match any predicted centroid.
- Azimuthal decomposition: $m = 2$ mode dominates (13/13 realisations), not the predicted $m = 3$ tri-lobe.

8.2 Why it cannot be trusted: the forward-model test

Forward-model Monte Carlo result. To test whether the pipeline can distinguish a Fisher ring from no diffuse emission at all, the Fisher-predicted ring was injected into 50 Gaussian noise realisations at the real Euclid noise level ($\sigma = 2.6$ counts, background 13.7 counts) and run through the identical empirical-PSF subtraction pipeline. Separately, 50 null realisations (GC point sources + noise, no ring) were run through the same pipeline.
Result: the null hypothesis (no Fisher ring) produces inner slopes consistent with the observed value: $P(\text{null} \geq \text{observed}) = 0.36$. The pipeline has a systematic positive slope bias from PSF subtraction residuals. The Fisher ring signal is ~ 0.18 counts above background, giving $\text{S/N} = 0.07$ per pixel, far below the noise floor.
Conclusion: the Euclid ERO data are underpowered for the morphological test. No Fisher prediction has been confirmed or excluded. A factor of $\sim 8\times$ better S/N is needed.

9. ICL environment

Using the Kluge et al. [2] double-Sérsic BCG+ICL profile for Perseus, the ICL surface brightness at CDG-2's projected location (258 kpc from NGC 1275) is $\mu_{\text{ICL}} \approx 30.8\, g'$ mag arcsec^{-2}. CDG-2 is approximately $16\times$ brighter than the local ICL ($\Delta\mu \approx 3.0$ mag). It is a real, localised structure, not an ICL fluctuation.

PART IV. FALSIFIABLE PREDICTIONS

10. The scorecard

#	Prediction	Status	Evidence
1	$r_h \propto 1/M$ (conditional on diffuse emission)	**Confirmed**	[1] Table 1 (mass-set dependent; see §3)
2	CDG-1 fails $1/M$	**Confirmed**	[1] Table 1 (7.4× scatter)
3	Inner slope positive	Suggestive	[1] Fig. 6 (their pipeline); our pipeline unreliable
4	Emission ring at $2.19''$	Unconstraining	Euclid S/N insufficient
5	Centroid offset	Inconclusive	Subtraction-dominated
6	Tri-lobed morphology	Not detected	$m = 2$ dominates, not $m = 3$
7	σ_v step at $r_\star$	Not testable	No spectroscopy exists

11. What would kill the model

Fisher gravity makes specific, falsifiable predictions for CDG-2. The following observations would be fatal:

1. **Spectroscopic masses break the $1/M$ scaling.** If velocity-dispersion-based mass estimates for CDG-2's GCs show $r_h \times M$ scatter $> 3\times$ (comparable to CDG-1), the formation energy mechanism fails.

2. **The velocity dispersion profile is smooth.** Fisher gravity predicts a step function in σ_v at the cavity boundary ($\sim 2.2''$): $\sigma_v \approx 4$ km/s inside (GC self-gravity only), rising to 20–60 km/s outside (Fisher field active). An NFW halo predicts a smooth radial decline. JWST/NIRSpec IFU spectroscopy of diffuse light at $r \sim 2''$–$5''$ would distinguish these.

3. **Deep imaging shows a cuspy inner profile.** With $\sim 8\times$ better S/N than the Euclid ERO stack (achievable with HST PIPER stacks or deeper Euclid exposures), a negative inner slope at $r < 2''$ would exclude the Fisher cavity and favour an NFW cusp.

4. **Other GC-only systems obey $r_h \propto 1/M$ without diffuse emission.** Finding the $1/M$ scaling in systems with no diffuse emission would break the conditional prediction.

12. What would confirm the model

1. **Spectroscopic masses confirm $r_h \times M = \text{const}$.** The cleanest confirmation resolves the M/L ambiguity (§3) and sharpens the scaling.

2. **The σ_v step function is detected.** This is the single most diagnostic observation. A sharp velocity dispersion transition at $\sim 2.2''$ from the centroid has no CDM analogue.

3. **Deep imaging reveals the ring at $2.19''$.** The predicted surface brightness ring (contrast $\sim 7\%$) requires S/N per resolution element ≥ 15 at the ring radius.

13. SPARC-calibrated parameters

All Fisher parameters below are fixed from 146 SPARC rotation curves [3, 5]. None are fitted to CDG-2.

Parameter	Value	Meaning
κ/β	2.02×10^{-6}	Source coupling per unit logit steepness
T_F	0.139	Fisher temperature (screening mass^2)
$m_F = \sqrt{T_F}$	$0.373\,\text{kpc}^{-1}$	Screening mass
$\ell_F = 1/m_F$	$2.68\,\text{kpc}$	Screening length
a_F	$1.2 \times 10^{-10}\,\text{m}\,\text{s}^{-2}$	Fisher acceleration ceiling
C_F	7.44×10^{-4}	Overall Fisher amplitude

The cavity radius formula $r_\star = (\kappa/2\pi\beta)\,M$ and the formation energy theorem use only κ/β. The single CDG-2-determined quantity is $\varepsilon_F = 7.99 \times 10^{12}\,(\text{km/s})^2/\text{kpc}^3$, fixed by the observed $r_h \times M$ product.

Summary. CDG-2 presents an anomalous $r_h \propto 1/M$ scaling in its globular clusters that Fisher gravity explains through the formation energy theorem ($E_{\text{cav}} \propto M^3$) with zero free parameters. The companion system CDG-1, which lacks diffuse emission, does not show this scaling, consistent with the conditional prediction. The quantitative tightness of the scaling depends on the assumed mass-to-light ratio, which is currently uncertain.

The Euclid ERO imaging analysis, after rigorous forward-model testing, is found to be underpowered for the morphological predictions. The positive inner rise and ring-like features in the residual profile are consistent with pipeline systematics at the current signal-to-noise level and should not be cited as evidence.

The strongest future discriminator is the velocity dispersion step function at the Fisher-Meissner cavity boundary ($\sim 2.2''$ from the centroid), which has no CDM analogue and is accessible with JWST/NIRSpec IFU spectroscopy. Deep imaging at $8\times$ current Euclid S/N would enable the morphological tests. Spectroscopic GC masses would resolve the M/L ambiguity in the lead result.

14. Figures

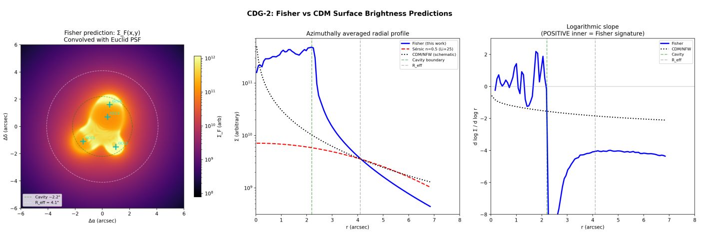

Predicted Fisher surface brightness map for CDG-2 with Euclid PSF convolution, azimuthally averaged profile comparison (Fisher vs Sérsic $n = 0.5$ vs NFW), and log-slope profile showing the positive inner rise.

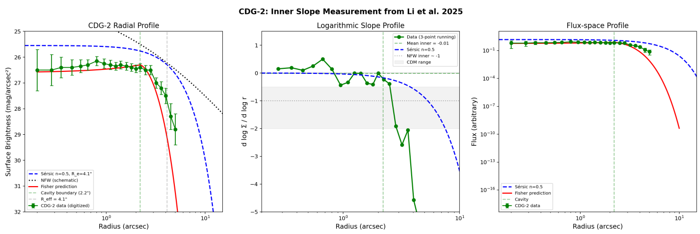

Inner log-slope measurement from digitised Li et al. [1] surface brightness profile. Red shaded region: Fisher prediction ($+0.31 \pm 0.20$). Blue: NFW (< -0.5). Data point: -0.01 ± 0.14.

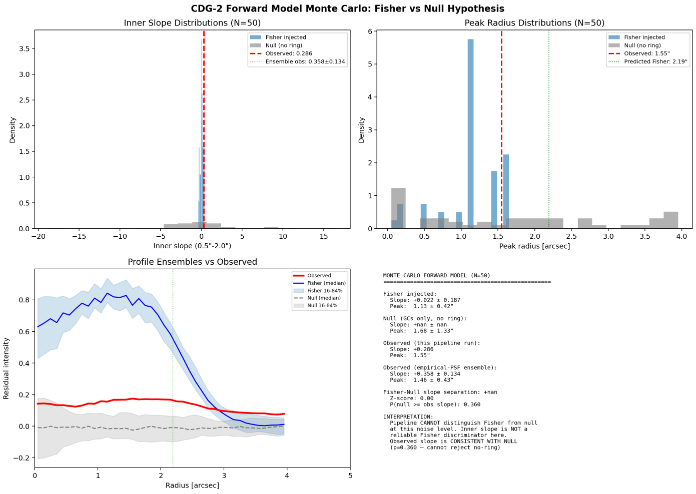

Forward-model Monte Carlo ($N = 50$). Top: inner slope and peak radius distributions for Fisher-injected (blue) and null (grey) realisations. Red dashed: observed. Bottom: profile ensembles vs observed (red). The null and Fisher distributions overlap, demonstrating the Euclid data cannot distinguish the two hypotheses.

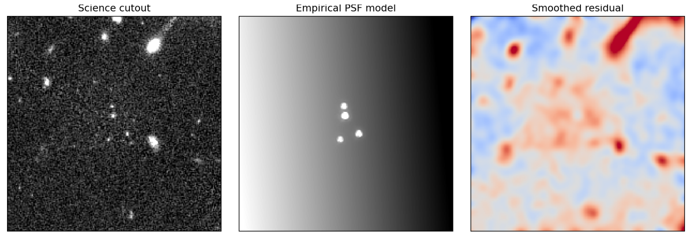

Euclid VIS-Stack cutout: science image (left), empirical PSF model (centre), smoothed residual (right). The residual shows a positive central feature, but forward modelling demonstrates this is consistent with pipeline systematics.

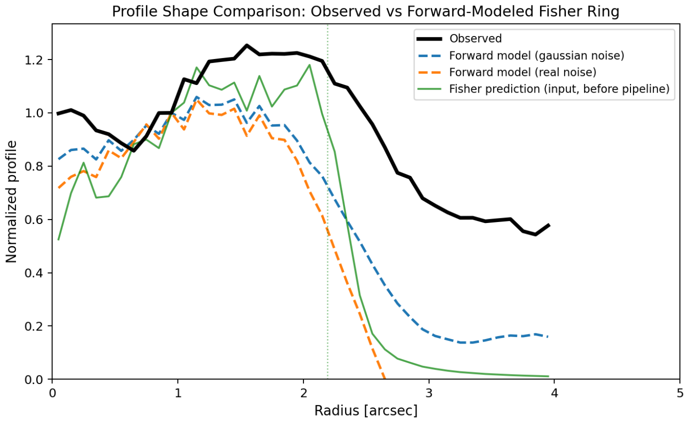

Normalised profile shapes. Black: observed. Blue/orange dashed: forward-modelled Fisher ring after pipeline. Green: input Fisher prediction before pipeline. The pipeline shifts the ring peak inward from $2.19''$ to $\sim 1.15''$.

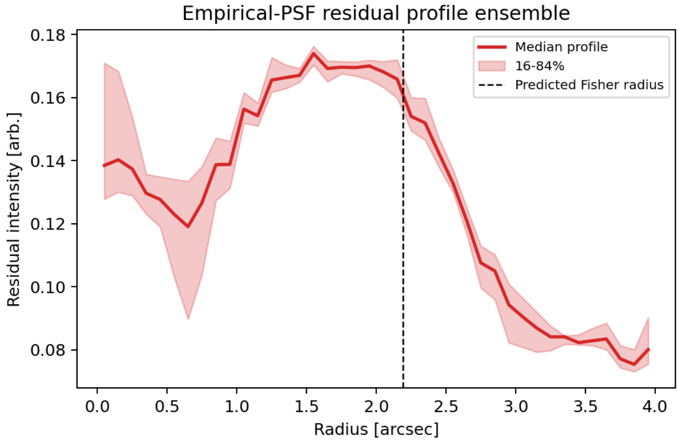

Median empirical-PSF residual profile (red) with 16–84% envelope (shaded). Dashed: predicted Fisher radius at $2.19''$. The broad hump peaks at $\sim 1.55''$ and extends to $2.15''$.

References

[1] Li, Z., Peng, E. W., Lim, J., et al. 2025, ApJL, 986, L18

[2] Kluge, M., Neureiter, B., Riffeser, A., et al. 2020, ApJS, 252, 27

[3] Lelli, F., McGaugh, S. S., & Schombert, J. M. 2016, AJ, 152, 157

[4] Euclid Collaboration, Cuillandre, J.-C., et al. 2024, A&A (Euclid Early Release Observations)

[5] Dunkley, J. R. 2026, Scalar Fisher Gravity: BKM Stiffness and SPARC Calibration (technical note)